Journal of Nuclear Materials 394 (2009) 34–38

Contents lists available at ScienceDirect

Journal of Nuclear Materials

journal homepage: www.elsevier.com/locate/jnucmat

Serrated flow behavior in AL6XN austenitic stainless steel

L.J. Meng, J. Sun *, H. Xing, G.W. Pang

School of Materials Science and Engineering, Shanghai Jiaotong University, Dongchuan Road 800, Shanghai 200240, PR China

ARTICLE INFO

Article history:
Received 14 January 2009
Accepted 4 August 2009

ABSTRACT

Serrated flow behavior of the AL6XN austenitic stainless steel has been investigated at different temperatures and strain rates. The results show the serrated flow, peak/plateau in flow stress and negative strain rate sensitivity appearing in tensile deformation of the AL6XN steel at 773–973 K and 3.3×10^{-5}–$3.3 \times 10^{-3}\,s^{-1}$ (excluding 873 K, $3.3 \times 10^{-5}\,s^{-1}$), suggesting the occurrence of dynamic strain aging (DSA). The activation energy for type-A and -(A + B) serrations was calculated to be 304 kJ/mol and diffusion of substitutional solutes, such as chromium and molybdenum is considered as the mechanism of serrated flow. TEM observations further revealed a typical planar slip mode in the regime of DSA of the deformed AL6XN steel.

1. Introduction

As one of the Generation IV nuclear reactors, a supercritical-water cooled reactor (SCWR) is being considered a candidate reactor because of its high thermal efficiency and simple design [1,2]. To meet the working circumstance of reactor core components of the supercritical-water cooled reactor, various properties, such as high tensile strength and creep strength at elevated-temperatures, low corrosion and stress-corrosion cracking susceptibility, good radiation resistance and weldability are required for materials of reactor core components. Three kinds of materials including ferrite/martensitic steel, austenitic stainless steel and nickel-base high-temperature alloy have been considered as potential materials used for reactor core components [3–5]. Austenitic stainless steels are usually known for their excellent corrosion resistance, high strength and exceptional toughness, ductility and formability. Among a variety of austenitic stainless steels, the AL6XN steel is a relatively new nitrogen-strengthened austenitic stainless steel developed by Allegheny Ludlum Corporation, and is distinguished by its more excellent corrosion and stress-corrosion resistance and elevated-temperature strength than those of types 304L and 316L stainless steels. Serrated flow, combined with negative strain rate sensitivity and peak/plateau in yield strength is often observed in the austenitic stainless steels, such as types 304L and 316L stainless steels. This phenomenon is also known as dynamic strain aging (DSA). Various physical models and micro-mechanism had been proposed to explain this phenomenon early [6–8], and it is widely accepted that dynamic strain aging arises from the interaction between diffusing solute atoms and mobile dislocations during plastic deformation and depends on the deformation rate and temperature, which govern the velocity of mobile dislocations and diffusing solute atoms. Dynamic strain aging has a significant influence on the mechanical properties, such as strength, ductility and low-cycle fatigue of materials [9–11]. Nasser et al. and Abed et al. have carried out studies on the plastic deformation theory and behavior of the AL6XN steel, respectively and serrated flow phenomenon has been found in the AL6XN steel at temperatures between 500 and 1000 K and at a strain rate of 0.001/s [12,13]. However, the serrated flow behavior of the AL6XN steel at elevated-temperatures received less attention. The purpose of this paper is to study the serrated flow behavior of the AL6XN austenitic stainless steel tensiled at temperatures of 773–973 K and at strain rates of 3.3×10^{-5}–$3.3 \times 10^{-3}\,s^{-1}$. The substructures of AL6XN after plastic deformation are observed by transmission electron microscopy (TEM). Additionally, the mechanism of plastic deformation of the AL6XN austenitic stainless steel at elevated-temperatures is discussed with the experimental results.

2. Experimental procedure

The cold-rolled AL6XN austenitic stainless steel supplied by Allegheny Ludlum Company was used for this study. The chemical composition of the AL6XN austenitic stainless steel is given in Table 1. All of specimens were solution-treated at 1393 K for 10 min followed by water quenching. The dog-bone specimens with a gauge length of 25 mm and a gauge diameter of 5 mm were fabricated for tensile tests. The tensile tests were carried out at room temperature and elevated-temperatures of 773–973 K and at strain rates of 3.3×10^{-5}–$3.3 \times 10^{-3}\,s^{-1}$ in air on Shimadzu AG-100KNA machine. The initial microstructure of solution-treated specimens was observed by scanning electron microscope (SEM) with electron backscattering diffraction (EBSD) attachment.

* Corresponding author. Tel.: +86 21 54745593; fax: +86 21 34203098.
E-mail address: jsun@sjtu.edu.cn (J. Sun).

0022-3115/$ - see front matter © 2009 Elsevier B.V. All rights reserved.
doi:10.1016/j.jnucmat.2009.08.002

Table 1
Chemical composition of the AL6XN austenitic stainless steel (wt.%).

C	Mn	P	S	Si	Cr	Ni	Mo	N	Cu	Fe
0.02	0.45	0.027	0.0002	0.32	20.31	23.87	6.20	0.20	0.36	Bal.

The samples for SEM observations were prepared by electro-polishing in a 20 vol.% perchloric acid, 10 vol.% glycerine and 70 vol.% ethanol solution. To examine the deformed substructures, the samples were also prepared by twin-jet electro-polishing in a 5 vol.% perchloric acid and 95 vol.% ethanol solution at 233–253 K and at 35 V for transmission electron microscope (TEM) observations. TEM observations were conducted on JEOL 2100F machine operating at 200 kV.

3. Results and discussion

The initial microstructure of solution-treated specimens was observed by scanning electron microscope (SEM) with electron backscattering diffraction (EBSD). The orientation imaging microstructure and inverse-pole figure of the solution-treated AL6XN austenitic steel are shown in Fig. 1. Equiaxed austenitic grains with an average diameter of 60 μm and with heavily annealing twins were observed, and no obviously preferred orientations were found in the solution-treated AL6XN steel.

Fig. 2 shows the engineering stress–strain curves obtained at room temperature and elevated-temperatures from 773 to 973 K at strain rates of 3.3×10^{-5}–3.3×10^{-3} s^{-1}. The serrated flow can be apparently observed on the stress–strain curves at 773–973 K and 3.3×10^{-5}–3.3×10^{-3} s^{-1} (excluding 873 K, 3.3×10^{-5} s^{-1}). The variation of tensile properties with temperatures at strain rate of 3.3×10^{-3} s^{-1} are presented in Table 2. The AL6XN austenitic stainless steel exhibits the highest 0.2% yield strength and ultimate tensile strength (UTS) at room temperature. However, the variation of 0.2% yield strength with temperatures remains nearly insensitive to the increase of deformation temperature from 773 to 923 K at strain rate of 3.3×10^{-3} s^{-1}. The ultimate tensile strength decreases slightly with increasing temperature. The tensile plasticity, percent elongation, of the AL6XN steel is substantial and does not change markedly at elevated-temperatures. The variation of normalized 0.2% yield strength and ultimate tensile strength (normalized with the elastic modulus) with temperatures from 773 to 973 K are further shown in Fig. 3. The elastic modulus used in this study at various temperatures are provided in Table 3, which were calculated in terms of the linear relationship between the elastic modulus and temperature of the AL6XN steel in the literature [14]. Fig. 3 shows an increasing trend of the normalized 0.2% yield strength with increasing temperatures from 773 to 973 K at strain rate of 3.3×10^{-3} s^{-1}, which shows anomalous behavior. The peak of the normalized ultimate tensile strength is achieved at 823–873 K at 3.3×10^{-3} s^{-1}. The strain rate sensitivity (SRS) parameters, m, were also calculated using the equation defined as

$$m = \log(\sigma_1/\sigma_2)/\log(\dot{\varepsilon}_1/\dot{\varepsilon}_2)$$

where σ_1 and σ_2 represent the flow stress at the different strain rate of $\dot{\varepsilon}_1$ and $\dot{\varepsilon}_2$, respectively. The SRS parameters of the AL6XN steel were obtained to be −0.052 and −0.054 at deformation temperatures of 823 and 873 K using the flow stresses at the strain rates of 3.3×10^{-4} s^{-1} and 3.3×10^{-3} s^{-1} and with the same 2% strain, respectively. The resulted tensile properties of serrated flow, peak/plateau in the flow stress and negative strain rate sensitivity indicate that the dynamic strain aging (DSA) occurs in the AL6XN steel tensile-deformed at 773–973 K and 3.3×10^{-5}–3.3×10^{-3} s^{-1} (excluding 873 K, 3.3×10^{-5} s^{-1}), which results from the interaction of mobile dislocations with the diffusing solute atoms. The locking dislocations from the atmospheres of solute atoms strengthen the resistance of deformation of the AL6XN steel.

The TEM micrograph of dislocation structure in the AL6XN steel tensile-deformed with true strain of 0.038 at 823 K and 3.3×10^{-4} s^{-1} is shown in Fig. 4. One can see that a typical planar slip mode exists in the regime of DSA for the AL6XN austenitic stainless steel, suggesting a strong interaction between the solute atoms and mobile dislocations. The fracture surface was observed by SEM for the AL6XN steel tensile-deformed at 873 K and 3.3×10^{-3} s^{-1}, which shows the occurrence of ductile rupture characterized by dimples, as shown in Fig. 5.

The different types of serrations appearing on the stress–strain curves follow the generally accepted nomenclature in the literatures [7,15]. Type-A serrations are periodic serrations from repeated deformation bands initiating at the same end and propagating in the same direction. These are locking serrations characterized by an abrupt rise in stress followed by a drop to or below the general level of the stress–strain curve. They occur in the low temperature or high strain rate part of the DSA regime. The type-B serrations are oscillations about the general level of the stress–strain curve that occur in quick succession due to discontinuous band propagation arising from the DSA of the moving dislocations within the Lüders band. Type-C serrations are yield drops below the general level of the stress–strain curve due to unlocking of the dislocations. Type-C serrations usually occur at higher temperatures or lower strain rates than types-A and -B serrations. The magnified views of different serrations of the true stress–strain curves are shown in Fig. 6. One can see that at strain rate of 3.3×10^{-3} s^{-1}, type-A serrations appear at 823 K and below, and type-(A + B) serrations at 873 and 923 K. Type-(A + B) serrations were also observed at 823 K, 3.3×10^{-5} s^{-1} and 3.3×10^{-4} s^{-1} and 873 K, 3.3×10^{-4} s^{-1}. Serrations disappeared at 873 K and 3.3×10^{-5} s^{-1}. Type-C serrations emerged after a certain strain at high-temperature of 973 K and at a strain rate of 3×10^{-3} s^{-1}. They became scarce with progressive deformation and finally disappeared at larger strain.

Serration flow always appears after a certain strain, critical plastic strain (ε_c), in DSA, which is dependent on both strain rate and temperature. The critical plastic strains were measured from the true stress–strain curves and a systematic trend was noticed in the variation of critical strain at 3.3×10^{-3} s^{-1} with temperatures, which is presented in Fig. 7. The onset of type-A and -(A + B) serrations, ε_c decreases with increasing temperature from 773 to 923 K, indicating the occurrence of the normal Portevin-Le Chatelier effect (PLE). However, the ε_c increases as type-C serrations appear at 923 K and 3×10^{-3} s^{-1}, which is the inverse PLE. In the inverse PLE region, the diffusion rates are high enough for dislocations to

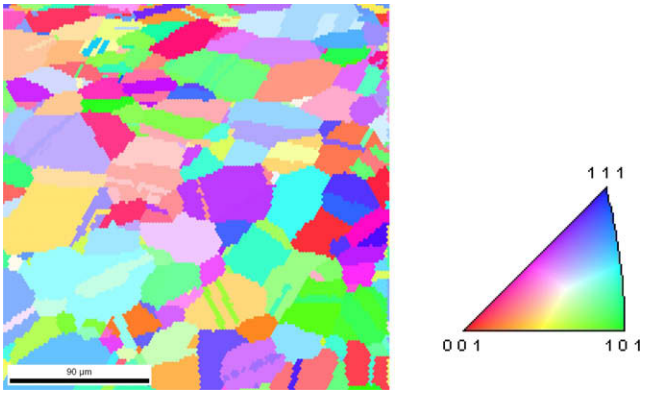

Fig. 1. Orientation imaging microstructure and inverse-pole figure in solution-treated steel.

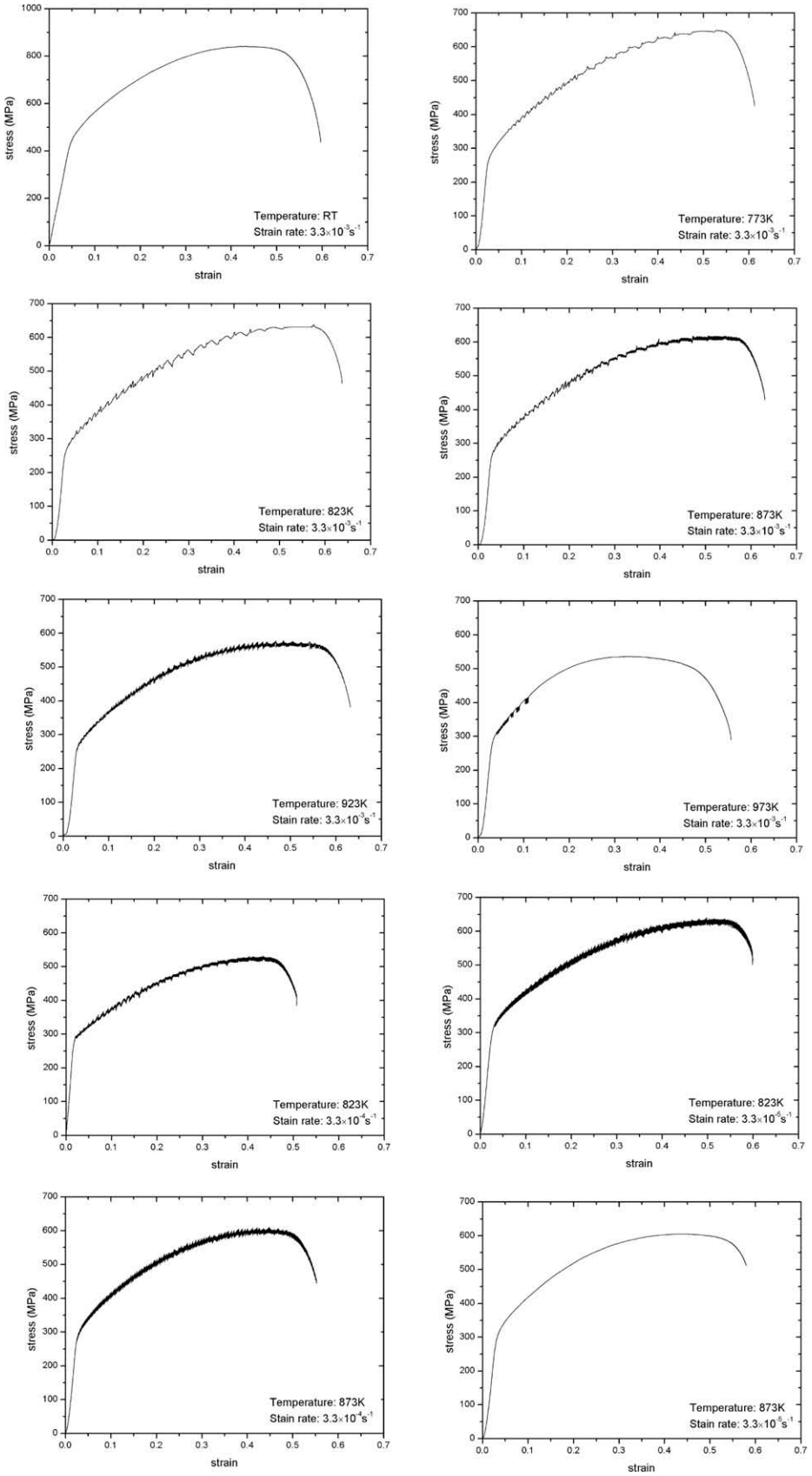

Fig. 2. Engineering stress–strain curves at different temperatures and strain rates.

be aged from the start of deformation, and type-C serrations appear to be due to breakaway of the aged dislocations [16]. It has been suggested that measurement of ε_c and its dependence on temperature and strain rate is essential to understand the

Table 2
Temperature dependence of tensile properties of the AL6XN steel.

	RT	773 K	823 K	873 K	923 K	973 K
$\alpha_{0.2}$ (MPa)	430.8	266.7	251.2	269.2	260.7	289.5
UTS (MPa)	840.5	648.8	637.4	618.9	576.4	535.7
δ (%)	55.1	55.3	59.9	59.0	59.3	52.5

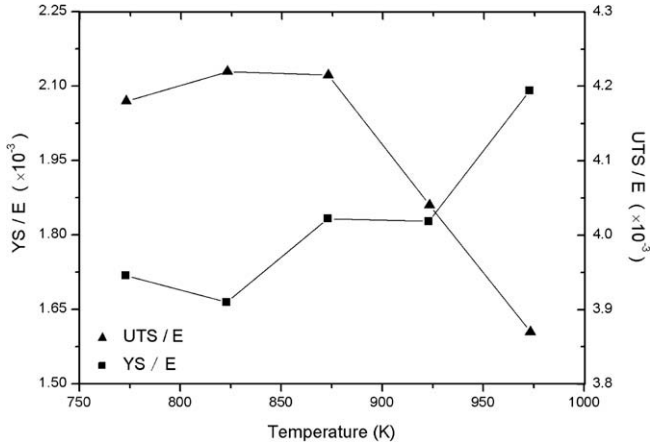

Fig. 3. Temperature dependence of normalized 0.2% yield strength and ultimate tensile strength at $3.3 \times 10^{-3}\ s^{-1}$.

Table 3
Temperature dependence of Young's modulus of the AL6XN steel.

Temperature (K)	297	773	823	873	923	973
E (GPa)	195	155.2	151.0	146.8	142.7	138.5

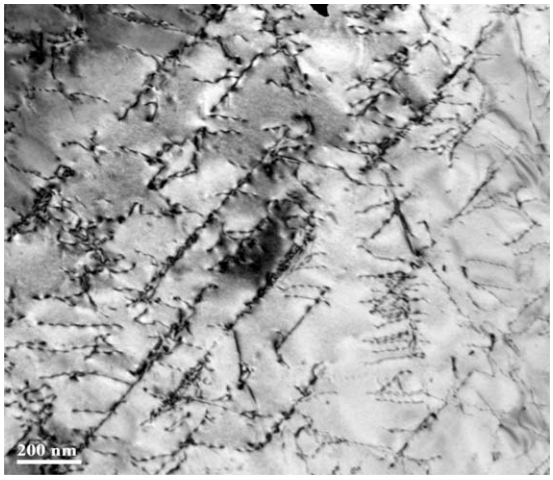

Fig. 4. TEM micrograph showing dislocation structure in the steel tested at 823 K and $3.3 \times 10^{-4}\ s^{-1}$.

underlying mechanism of DSA [7]. This dependence is generally expressed as

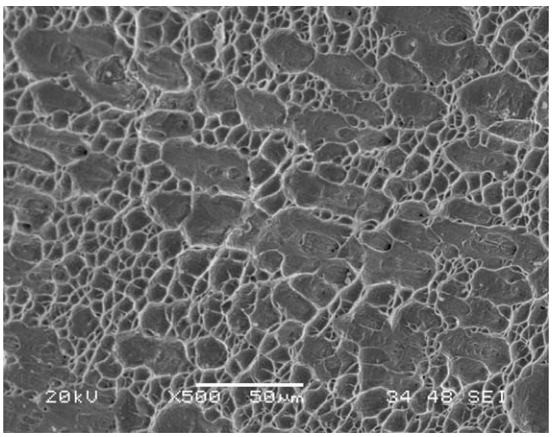

Fig. 5. Fractograph of the steel fractured at 873 K and $3.3 \times 10^{-3}\ s^{-1}$.

$$\varepsilon_c^{m+\beta} = K\,\dot{\varepsilon}\,\exp(Q/kT)$$

where m and β are the respective exponents related to the vacancy concentration and mobile dislocation density respectively, K the constant, $\dot{\varepsilon}$ the strain rate, Q the activation energy, k the Boltzmann constant, T the absolute temperature. The average $(m+\beta)$ value as estimated to be 2.4 from the critical plastic strains measured at different temperatures and strain rates. With the $(m+\beta)$ value, activation energy was further calculated to be 304 kJ/mol for type-A and -(A + B) serrations at temperatures ranging from 773 to 923 K, as shown in Fig. 8. Tamhankar et al. derived a value of activation energy for serrated flow in the 10Cr–35Ni–0.39Mn–0.03C alloy as 210–340 kJ/mol [17]. By taking $(m+\beta)$ equals 2.3, Mannan et al. and Samuel et al. also calculated the activation energy for serrated flow at elevated-temperatures in AISI type 316 stainless steels as 255 and 277 kJ/mol, respectively [18,19]. Almeida et al. reported the activation energy derived from the critical strain for type-B serrations as 240 kJ/mol in the type 304 stainless steel [20]. The value of 304 kJ/mol for the activation energy of serrated flow in the AL6XN steel is comparable with those reported in the austenitic stainless steel in the literature. This tends to support that diffusion of substitutional solute atoms is responsible for serrated flow in the AL6XN austenitic steel at elevated-temperatures. Additionally, the $(m+\beta)$ value for the AL6XN steel falls into the range between 2 and 3, again indicating a substitutional diffusion-controlled mechanism of DSA [7]. Thus, the diffusion of substitutional solutes, such as chromium and molybdenum is considered as the mechanism of serrated flow of the AL6XN austenitic steel.

4. Conclusions

Tensile tests were conducted on the solution-treated AL6XN austenitic stainless steel at temperatures of 773–973 K and at strain rates of 3.3×10^{-5}–$3.3 \times 10^{-3}\ s^{-1}$. Based on the results, the conclusions were made as follows:

(1) During tensile deformation at temperature ranging from 773 to 973 K and at strain rates of 3.3×10^{-5}–$3.3 \times 10^{-3}\ s^{-1}$ (excluding 873 K, $3.3 \times 10^{-5}\ s^{-1}$), the regime of DSA was manifested by the serrated flow, peak/plateau in flow stress and negative strain rate sensitivity. Additionally, type-A and -(A + B) serrations were identified at relatively low temperatures, whereas type-C serrations were observed at higher temperature.

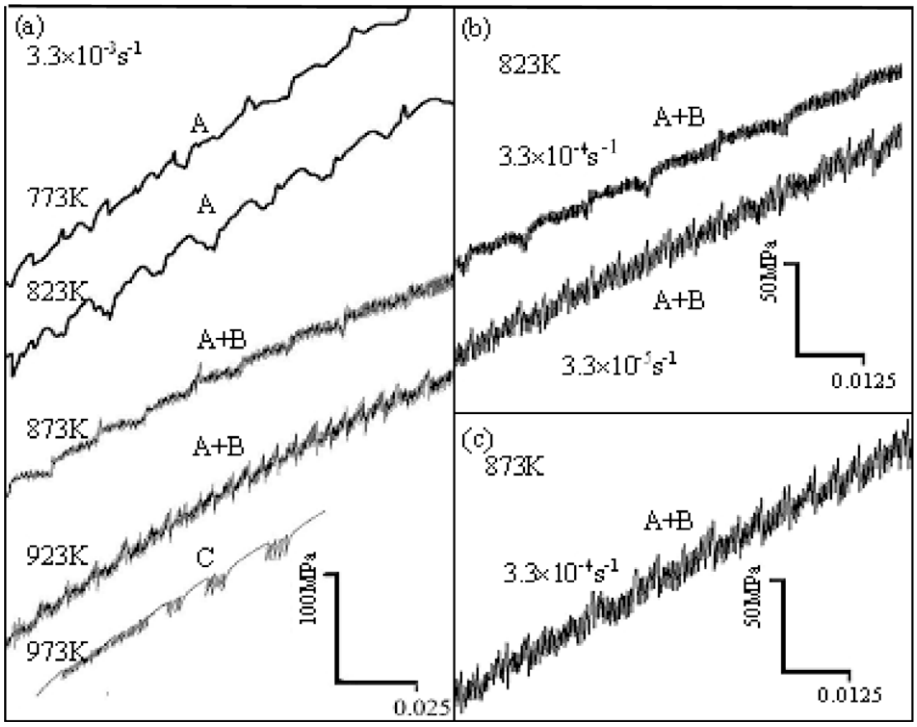

Fig. 6. Magnified view of serrations of true stress–strain curves: (a) 773–973 K, $3.3 \times 10^{-3}\ s^{-1}$; (b) 823 K, $3.3 \times 10^{-4}\ s^{-1}$–$3.3 \times 10^{-5}\ s^{-1}$; (c) 873 K, $3.3 \times 10^{-4}\ s^{-1}$.

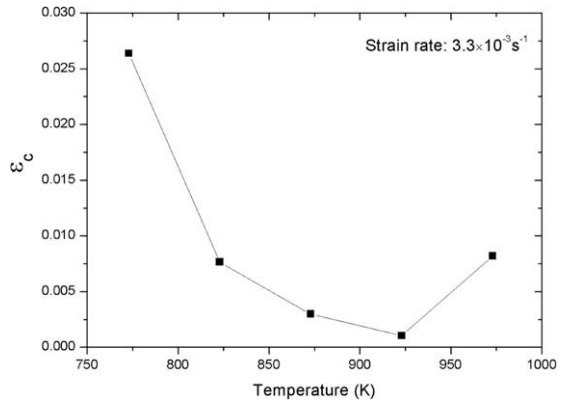

Fig. 7. Plot of critical strain of serrations with different temperatures at $3.3 \times 10^{-3}\ s^{-1}$.

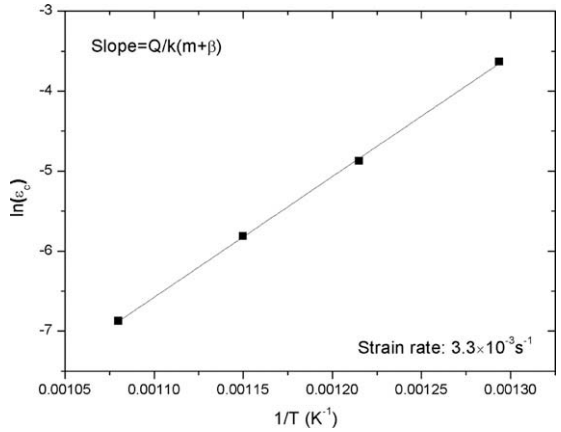

Fig. 8. Plot of critical strain vs. $1/T$.

(2) The critical strains for type-A and -(A + B) serrations were determined, which decreases with increasing temperature from 773 to 923 K. The value of activation energy for serrated flow was calculated to be 304 kJ/mol, and diffusion of substitutional solutes, such as chromium and molybdenum is considered as the mechanism of DSA.

Acknowledgement

This work is financially supported by National Basic Research Program of China (Project No. 2007CB209803).

References

[1] K. Kataoka et al., Proc. ICAPP' 03 (2003) 4.
[2] D. Squarer, T. Schulenberg, D. Struwe, Y. Oka, D. Bittermann, N. Aksan, C. Maraczy, R. Kyri-Rajamäki, A. Souyri, P. Dumaz, Nucl. Eng. Des. 221 (2003) 167.
[3] K. Ehrlich, J. Konys, L. Heikinheimo, J. Nucl. Mater. 327 (2004) 140.
[4] G.S. Was, P. Ampornrat, G. Gupta, S. Teysseyre, E.A. West, T.R. Allen, K. Sridharan, L. Tan, Y. Chen, X. Ren, C. Pister, J. Nucl. Mater. 371 (2007) 176.
[5] S.S. Hwang, B.H. Lee, J.G. Kim, J. Jang, J. Nucl. Mater. 372 (2007) 177.
[6] P.G. Mccormick, Acta Metall. 20 (1972) 351.
[7] P. Rodriguez, Bull. Mater. Sci. 6 (1984) 653.
[8] S.D. Mesarovic, J. Mech. Phys. Solids 43 (1995) 671.
[9] D.W. Kim, W.G. Kim, W.S. Ryu, Int. J. Fatigue 25 (2003) 1203.
[10] S.G. Hong, K.O. Lee, S.B. Lee, Int. J. Fatigue 27 (2005) 1420.
[11] M.H. Lee, J.H. Kim, B.K. Choi, Y.H. Jeong, J. Alloys Compd. 428 (2007) 99.
[12] S.N. Nasser, W.G. Guo, D.P. Kihl, J. Mech. Phys. Solids 49 (2001) 1823.
[13] F.H. Abed, G.Z. Voyiadjis, Int. J. Plasticity 21 (2005) 1618.
[14] AL6XN Alloy (UNS N08367), Allegheny Technologies, Allegheny Ludlum Corporation, 2002, p. 28.
[15] B. Russell, Philos. Mag. 8 (1963) 615.
[16] W. Charnock, Philos. Mag. 20 (1969) 209.
[17] R. Tamhankar, J. Pleteau, C. Crussard, Rev. Met. 55 (1958) 383.
[18] S.L. Mannan, K.G. Samuel, P. Rodriguez, Trans. Indian Instrum. Met. 36 (1983) 313.
[19] K.G. Samuel, S.L. Mannan, P. Rodriguez, Acta Met. 36 (1987) 2323.
[20] L.H. Almeida, P.R.O. Emygdio, Scr. Metall. Mater. 31 (1994) 505.